PROCEEDINGS OF SPIE

SPIEDigitalLibrary.org/conference-proceedings-of-spie

Optomechanical analysis of compliant spacers in passively athermalized drop-in optical systems

Martin Tangari Larrategui, Victor Densmore, Lee Johnson, Christian Baker, Matthew Hevert, et al.

Martin Tangari Larrategui, Victor E. Densmore III, Lee Johnson, Christian Baker, Matthew Hevert, Bianka Camacho, Paul Tulungen, Peter McNiven, Kate Medicus, Kenneth R. Castle, Tilman W. Stuhlinger, "Optomechanical analysis of compliant spacers in passively athermalized drop-in optical systems," Proc. SPIE 12222, Optical System Alignment, Tolerancing, and Verification XIV, 122220A (3 October 2022); doi: 10.1117/12.2633612

SPIE.

Event: SPIE Optical Engineering + Applications, 2022, San Diego, California, United States

Optomechanical analysis of compliant spacers in passively athermalized drop-in optical systems

Martin Tangari Larrategui*[a], Victor E. Densmore III [a], Lee Johnson [a], Christian Baker [a], Matthew Hevert [a], Bianka Camacho [a], Paul Tulungen [a], Peter Mc. Niven [a], Kate Medicus [a], Kenneth R. Castle [a], Tilman W. Stuhlinger [a]

[a] Ruda Cardinal Inc., 3280 E. Hemisphere Loop, #180, Tucson, AZ 85706

ABSTRACT

Passively athermalized optical systems produce high quality images over a large thermal range without actively adjusting focus. This athermalization is achieved through careful selection of the glass for each lens and metal for each mount. For drop-in systems, the material combination for best optical performance often leads to a lens stack with an overall coefficient of thermal expansion (CTE) that is different from the CTE of the barrel that holds it together. Since bulk glass and metal are relatively stiff, this CTE mismatch results in large variations of the preload force retaining the lens stack in compression over the optical system's survival thermal range. For this reason, compliant spacers are commonly added to the lens stack in an effort to attenuate these preload force variations. However, the effect of these compliant spacers on the athermalization of optical systems is seldom analyzed. We perform a first-order calculation of the effective CTE of compliant spacers to assess their impact on optical performance and introduce an optomechanical design approach to reduce the amount of compliance needed by matching the overall CTE of the lens stack to the CTE of the barrel.

Keywords: Athermalization, compliance, coefficient of thermal expansion, preload force, contact stress, optical design

1. INTRODUCTION

The effects of environmental changes on the performance of optical systems have been discussed extensively in the literature. Pressure variations affect the refractive index of air, resulting in a small change in the relative refractive index of all glasses [1, 2]. Thermal variations affect the refractive index of air and glasses, as well as the length of all mechanical features (radii of curvature, thicknesses, diameters, etc.) [3]. These effects alter the power and position of all optical surfaces, leading to a first order change in focus (i.e., a displacement between the image plane and the detector location). For this reason, imaging systems that were compensated for focus at a nominal temperature and pressure may be out of focus at different environmental conditions. This focus change can be mitigated by placing the detector on a motorized stage that repositions it to the image plane (active athermalization) or by leveraging the existing/available glasses and metals to design an optical system that produces an image at the detector location for all environmental conditions (passive athermalization).

The position of optical surfaces is also affected by the optical system's mounting geometry. For instance, the variation with temperature of the vertex to vertex spacing between two lenses is different for drop-in mounting (spacer contacting the right surface of the first lens and the left surface of the second lens) than seat mounting (cell/barrel contacting the right surface of the first lens and the right surface of the second lens). Furthermore, if the mount contacts the lens on an optical surface, the contact height varies with temperature according to the CTE of the metal. If it contacts the lens on an annulus, it varies according to the CTE of the glass. Each of these permutations leads to a different vertex to vertex spacing between lenses.

Optical engineers must therefore model the mechanical features that control the position of optical surfaces at the operational environmental conditions. However, all other mechanical features that do not influence optical performance are rarely modelled in optical design software. In this paper, we highlight the benefits of considering the effects of the barrel material in the design of passively athermalized drop-in systems. We calculate the ideal barrel CTE based on the overall CTE of the lenses and spacers in the stack, and the effective CTE of compliant spacers based on the actual material of the barrel. We then analyze their impact on the polychromatic MTF at different environmental conditions and introduce an optimization procedure to reduce the amount of compliance needed and therefore minimize its effect on optical performance.

Optical System Alignment, Tolerancing, and Verification XIV, edited by José Sasián, Richard N. Youngworth, Proc. of SPIE Vol. 12222, 122220A · © 2022
SPIE · 0277-786X · doi: 10.1117/12.2633612

2. SPECIFICATIONS AND OPTICAL DESIGN

We illustrate this technique with an aerospace vacuum lens designed to the following specifications:

- 100 mm focal length (at $\lambda = 0.675$ µm, P = 0 atm and $T_o = 20°C$)
- F/2.8 (≈ 35.71 mm entrance pupil diameter at $T_o = 20°C$)
- 28 mm image diameter (APS-C sensor)
- Broadband spectrum defined as: $\lambda_1 = 0.450$ µm (0.33 weight), $\lambda_2 = 0.563$ µm (0.78 weight), $\lambda_3 = 0.675$ µm (0.89 weight), $\lambda_4 = 0.788$ µm (1.00 weight), and $\lambda_5 = 0.900$ µm (0.56 weight)
- 200°C thermal range ($T_{min} = -80°C$, $T_o = 20°C$ and $T_{max} = 120°C$)
- $P_o = 0$ atm (space vacuum)
- Minimum of radial and tangential polychromatic MTF at 100 lp/mm (for the defined wavelengths and weights) must be greater than 40% for all field locations over the thermal range
- Maximum $f \cdot \tan(\theta)$ distortion must be smaller than 1% over the thermal range
- TFL mount (M35x0.75 mm thread with a 17.526 mm flange distance)
- Outer diameter of lens barrel must be smaller than 50 mm
- Overall length from the detector to the front surface of the barrel must be smaller than 120 mm
- Lens must survive 10 g's of axial and radial acceleration
- First lens must be made from a radiation resistant glass (Ohara S-BSL7R, S-BAL35R, S-BSM22R, etc.)
- No vignetting

We adapted the lens specifications and design from Rogers [4] for drop-in assembly to showcase the impact of compliant spacers on the optical performance at different environmental conditions. Figure 1 shows the optical design layout of the initial design and Figure 2 shows its polychromatic MTF at $T_{min} = -80°C$, $T_o = 20°C$ and $T_{max} = 120°C$.

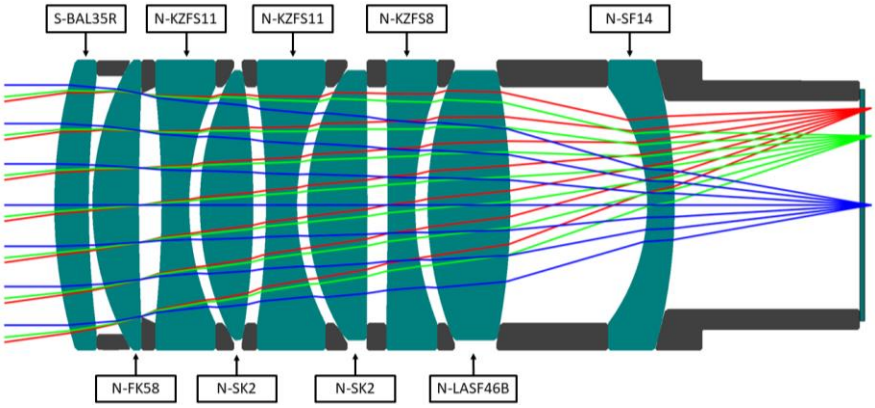

Figure 1. Optical design layout of the initial design with 6061-T6 aluminum spacers.

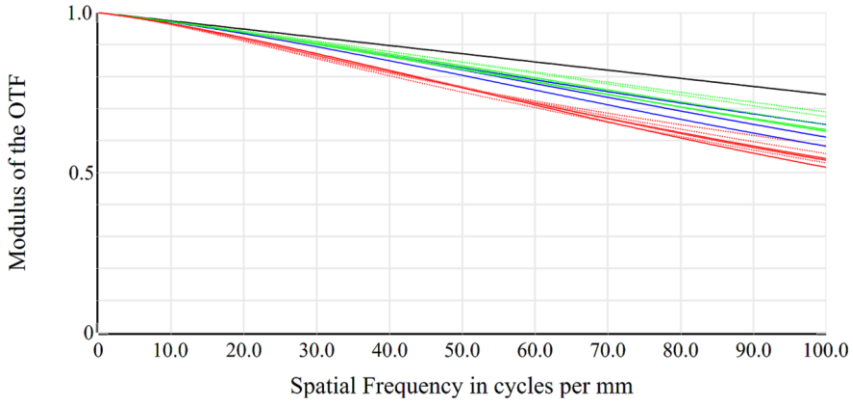

Figure 2. Polychromatic MTF overlay of the initial design for $T_{min} = -80°C$, $T_o = 20°C$ and $T_{max} = 120°C$. Blue, green, and red curves represent the on-axis, 70% and 100% fields of view, respectively.

3. DROP-IN MECHANICAL DESIGN

Figure 3 shows the drop-in mechanical design layout. Its assembly process consists of threading the detector interface to the back of the barrel, dropping the individual lenses and spacers from back to front (using a vacuum cup), tapping the barrel so the lenses self-align, and threading the retaining ring in the front (to a specified preload) to hold everything together. The radial clearance between the inner diameter (ID) of the barrel and the outer diameter (OD) of the lenses and spacers controls the centration of the composing elements in the stack. Since this clearance must be greater than zero at the lowest survival temperature to prevent radial stress on the lenses, drop-in mounting can only hold relatively loose centration tolerances.

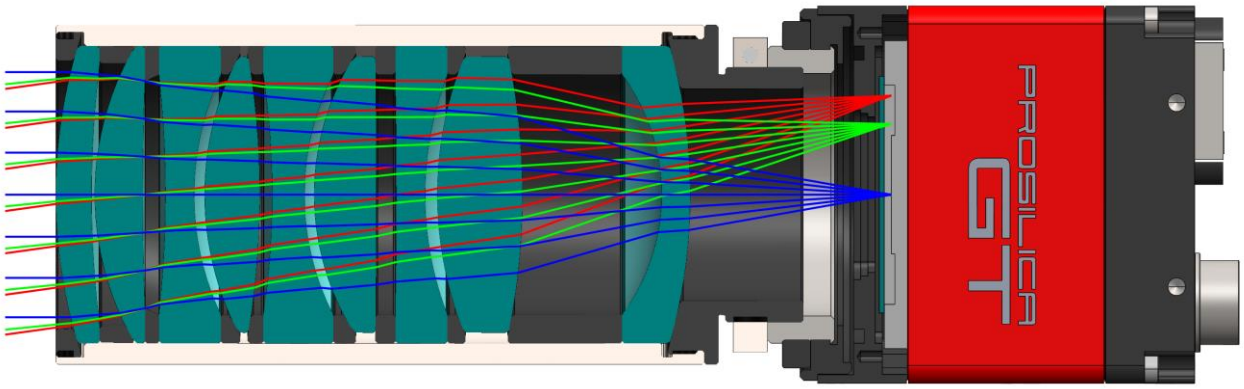

Figure 3. Mechanical design layout. The blue, green and red rays represent the on-axis, 70% and 100% fields of view, respectively. Since the circular image overfills the rectangular detector, the green and red rays converge outside the detector area in this section view.

Despite this limitation, drop-in mounting is one of the few assembly approaches that allows for the OD of the optical system to be only slightly larger than its entrance pupil diameter (EPD). This is because the aperture stop in optical systems designed around this requirement is commonly placed towards the front of the lens, leading to composing elements of similar OD. Drop-in mounting these elements in a barrel only adds the thin wall thickness of the barrel to the clear OD of the optical system, minimizing the total volume.

After establishing the mechanical design, we calculated the minimum preload to retain the lenses under axial acceleration P_{AXIAL} at the nominal assembly temperature (T_o = 20°C) through Equation 3.1 [5]:

$$P_{AXIAL} = a_G \sum_{i=1}^{n} W_i, \tag{3.1}$$

where a_G = 10·(9.81 m/s^2) is the specified acceleration, and W = 0.298 Kg is the overall mass of the lens stack (computed as the sum of the masses of the individual lenses and spacers W_i). We then calculated the minimum preload to retain each lens under radial acceleration P_{RADIAL} at T_o = 20°C through Equation 3.2 [5]:

$$P_{RADIAL} = \left(\frac{Wa_G}{\mu}\right)\cos^2\left(-\arcsin\left(\frac{y_1}{R_1}\right)+\arcsin\left(\frac{y_2}{R_2}\right)\right), \tag{3.2}$$

where μ = 0.2 is the estimated static friction coefficient of the glass/metal interface, y_1 and y_2 are the radial lens/spacer contact heights, and R_1 and R_2 are the radii of curvature of each surface. We summarized the minimum preloads to retain each lens under radial acceleration in Table 1.

Since P_{AXIAL} = 29.3 N and $(P_{RADIAL})_{MAX}$ = 17.5 N, a P = 45 N preload can retain the lenses under 10g's of acceleration at the nominal assembly temperature with a factor of safety $FS \approx 1.5$. When the axial acceleration is in the opposite direction of the preload, the lenses are retained under $P_{MIN} = P - P_{AXIAL}$ = 45 N – 30 N = 15 N. When the axial acceleration is in the same direction as the preload, the lenses are retained under $P_{MAX} = P + P_{AXIAL}$ = 45 N + 30 N = 75 N.

The contact stress on each surface under the maximum preload P_{MAX} for a tangential/conical interface between the spacers and convex optical surfaces $\sigma_{TANGENTIAL}$ is given by [5]:

$$\sigma_{TANGENTIAL} = 0.798\sqrt{\left(\frac{P_{MAX}}{2\pi y_C}\right)\left(\frac{1}{2R}\right)\frac{1}{\left(\frac{1-\nu_{LENS}{}^2}{E_{LENS}}+\frac{1-\nu_{SPACER}{}^2}{E_{SPACER}}\right)}}, \tag{3.3}$$

where ν_{LENS}, ν_{SPACER}, E_{LENS} and E_{SPACER} are the Poisson ratios and Young's moduli for the lenses and spacers, respectively. The tangential contact stresses for each surface (assuming ν_{SPACER} = 0.33 and E_{SPACER} = 68,900 MPa for 6061-T6 aluminum spacers), and respective factors of safety *FS* for a maximum allowable compressive stress of σ_{MAX} = 345 MPa (FS = $\sigma_{MAX}/\sigma_{TANGENTIAL}$) are summarized in Table 2.

Table 1. Minimum preload to retain each lens under radial acceleration computed with Equation 3.2 based on the lens type, mass *W*, lens/spacer contact heights y_1 and y_2, and lens radii of curvature R_1 and R_2.

Lens	Type	W [g]	y_1 [mm]	R_1 [mm]	y_2 [mm]	R_2 [mm]	P_{RADIAL} [N]
1S	Meniscus	19.066	20.000	73.063	18.500	∞ (Annulus)	8.7
2S	Meniscus	21.251	19.750	41.676	17.000	∞ (Annulus)	8.1
3S	Biconcave	31.686	17.000	∞ (Annulus)	17.000	∞ (Annulus)	15.5
4S	Biconvex	19.539	18.500	42.223	18.500	-118.794	6.4
5S	Biconcave	35.769	17.000	∞ (Annulus)	17.000	∞ (Annulus)	17.5
6S	Biconvex	25.287	18.500	36.705	18.500	-1574.081	9.1
7S	Biconcave	27.726	17.000	∞ (Annulus)	17.000	∞ (Annulus)	13.6
8S	Biconvex	49.326	18.500	52.091	18.500	-98.196	17.5
9S	Meniscus	27.088	17.000	∞ (Annulus)	18.500	-77.657	12.5
						Max	**17.5**

Table 2. Contact stress at the tangential lens/spacer interfaces computed with Equation 3.3 for a P_{MAX} = 75 N force applied at the contact height y_C on the lenses with Poisson ratio ν_{LENS}, Young's modulus E_{LENS}, and radius of curvature *R*.

Surface	Material	ν_{LENS}	E_{LENS} [MPa]	R [mm]	y_C [mm]	$\sigma_{TANGENTIAL}$ [MPa]	FS
1S_s1	S-BAL35R	0.255	83,000	73.063	20.000	10.4	33.3
2S_s1	N-FK58	0.301	70,000	41.676	19.750	13.3	25.9
4S_s1	N-SK2	0.263	78,000	42.223	18.500	14.0	24.7
4S_s2	N-SK2	0.263	78,000	-118.794	18.500	8.3	41.4
6S_s1	N-SK2	0.263	78,000	36.705	18.500	15.0	23.0
6S_s2	N-SK2	0.263	78,000	-1574.081	18.500	2.3	150.6
8S_s1	N-LASF46B	0.303	121,000	52.091	18.500	13.9	24.8
8S_s2	N-LASF46B	0.303	121,000	-98.196	18.500	10.1	34.1
9S_s2	N-SF14	0.259	88,000	-77.657	18.500	10.6	32.5
						Min	**23.0**

4. ENVIRONMENTAL EFFECTS

The minimum preload to retain the lenses under the specified acceleration at T_o = 20°C is independent of the barrel material. As the temperature changes, the barrel expands and contracts according to its material CTE (α_{BARREL}), and the stack of lenses and spacers expands and contracts according to its overall stack CTE (α_{STACK}). When these coefficients of thermal expansion are not equal ($\alpha_{STACK} \neq \alpha_{BARREL}$), the differential expansion rate leads to a change in preload ΔP, which is computed through Equation 4.1 [5]:

$$\Delta P = K_3 \Delta T, \tag{4.1}$$

where ΔT = 100°C is the difference between the nominal and maximum survival temperatures (same as the maximum operating temperature for this design), and K_3 is the rate at which the preload changes with temperature. The overall stack

CTE (α_{STACK}), which is equal to the ideal barrel CTE for no change in preload under thermal variations, is given by Equation 4.2:

$$\alpha_{STACK} = \frac{\sum_{i=1}^{n} \alpha_i t_i}{\sum_{i=1}^{n} t_i}, \tag{4.2}$$

where t_i is the length of the individual lenses and spacers at their contact height (different from the lens spacing and center thickness), and α_i are the respective CTEs of the lenses and spacers. K_3 is computed through Equation 4.3 [5]:

$$K_3 = \frac{-\sum_{i=1}^{n} (\alpha_{BARREL} - \alpha_i)(t_i)}{\sum_{i=1}^{n} C_i} = \frac{(\alpha_{STACK} - \alpha_{BARREL}) \sum_{i=1}^{n} t_i}{\sum_{i=1}^{n} C_i}, \tag{4.3}$$

where the numerator is the rate of differential expansion between the barrel and the stack, and the denominator is the sum of the bulk compliances C_i of the barrel and all the lenses and spacers in the stack. The bulk compliance (inverse stiffness) of each element depends on its material, diameter, radial contact height with the preceding and following elements in the stack and thickness at the contact height. It is independent of radius of curvature of the optical surfaces and the angle of the tangential lens/spacer interfaces. The bulk model layout of the drop-in mechanical design is shown in Figure 4.

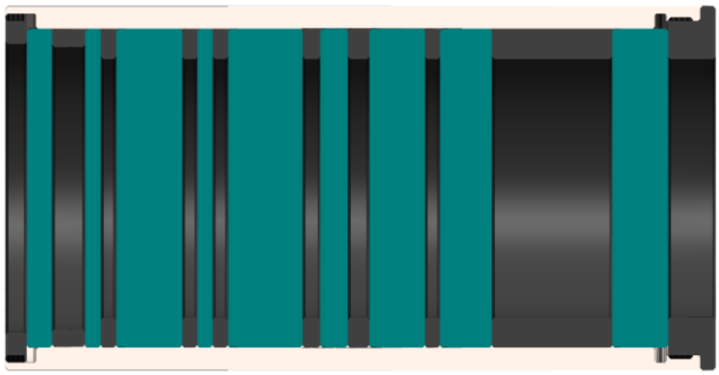

Figure 4. Bulk model layout of the mechanical design. The lenses are modelled as cylinders with the same OD as the non-bulk lens. The spacers are modelled as hollow cylinders with the same OD and ID as the non-bulk spacers, and thickness equal to the thickness at the contact height.

The bulk compliances C_i of each element can be estimated through finite element analysis (FEA) or approximated analytically based on equations derived from general FEA cases [6] as shown in Equations 4.4 through 4.7. The bulk compliance of lenses is given by Equation 4.4 [5]:

$$C_{LENS} = \frac{2t_L}{E_L A_L}, \text{ where } A_L = \begin{cases} 2\pi y_C t_L & \text{for } (2y_C + t_L) < OD_L \\ \frac{\pi}{4}\left(OD_L{}^2 - (2y_C - t_L)^2\right) & \text{for } (2y_C + t_L) \geq OD_L \end{cases} \tag{4.4}$$

y_C is the contact height, t_L is the thickness of the lens at the contact height, and OD_L is the outer diameter of the lens. The bulk compliance of the barrel is given by Equation 4.5 [5]:

$$C_{BARREL} = \frac{t_B}{E_B A_B}, \text{ where } A_B = \pi t_W (ID_B + t_W), \tag{4.5}$$

t_W is the wall thickness of the barrel, ID_B is the inner diameter of the barrel, and t_B is the length of the barrel from the contact height of the first optical surface to the contact height of the last optical surface. The bulk compliance of a spacer is given by Equations 4.6 and 4.7 [5]:

$$C_{SPACER} = \frac{t_S}{E_S A_S}, \text{ where} \tag{4.6}$$

$$A_S = \begin{cases} 2\pi\left[\frac{OD_S}{2} - \frac{1}{2}\left(\frac{OD_S}{2} - \frac{y_{C_1} + y_{C_2}}{2}\right)\right]\left(\frac{OD_S}{2} - \frac{y_{C_1} + y_{C_2}}{2}\right) & \text{flat/flat contact} \\ 2\pi\left[\frac{OD_S}{2} - \frac{1}{2}\left(\frac{OD_S}{2} - \frac{y_{C_1} + 2y_{C_2}}{2} + \frac{OD_{G_2}}{4}\right)\right]\left(\frac{OD_S}{2} - \frac{y_{C_1} + 2y_{C_2}}{2} + \frac{OD_{G_2}}{4}\right) & \text{flat/tangential contact} \\ 2\pi\left[\frac{OD_S}{2} - \frac{1}{2}\left(\frac{OD_S}{2} - \frac{2y_{C_1} + 2y_{C_2}}{2} + \frac{OD_{G_1} + OD_{G_2}}{4}\right)\right]\left(\frac{OD_S}{2} - \frac{2y_{C_1} + 2y_{C_2}}{2} + \frac{OD_{G_1} + OD_{G_2}}{4}\right) & \text{tangential/tangential contact} \end{cases} \tag{4.7}$$

y_{C1} and y_{C2} are the lens/spacer contact heights, OD_{G1} and OD_{G1} are the outer diameters of the lenses, t_S is the thickness of the spacer at the contact height, E_S is the Young's modulus of the spacer, and OD_S is the outer diameter of the spacer. For this drop-in mechanical design, the bulk compliance of a 6061-T6 aluminum barrel is:

$$C_{BARREL} = \frac{(84.691\text{ mm})}{(68{,}900\text{ N/mm}^2)\pi(2.95\text{ mm})(42.1\text{ mm} + 2.95\text{ mm})} = 2.9\text{x}10^{-6}\text{ mm/N}. \tag{4.8}$$

The bulk compliance of the lenses and spacers are summarized in Tables 3 and 4, respectively.

Table 3. Bulk compliance of the lenses in the stack computed with Equation 4.4.

Lens	Material	E_{LENS} [MPa]	t_{LENS} [mm]	y_C [mm]	$2y_C + t_{LENS}$ [mm]	OD_{LENS} [mm]	C_{LENS} [mm/N]
1S	S-BAL35R	83,000	3.355	20.000	43.355	42.000	$2.4\text{x}10^{-7}$
2S	N-FK58	70,000	2.110	19.750	41.610	42.000	$2.1\text{x}10^{-7}$
3S	N-KZFS11	79,000	8.725	18.500	45.725	42.000	$2.9\text{x}10^{-7}$
4S	N-SK2	78,000	2.032	18.500	39.032	39.000	$2.2\text{x}10^{-7}$
5S	N-KZFS11	79,000	9.862	18.500	46.862	42.000	$3.1\text{x}10^{-7}$
6S	N-SK2	78,000	3.638	18.500	40.638	39.000	$2.9\text{x}10^{-7}$
7S	N-KZFS8	103,000	7.359	18.500	44.359	42.000	$2.1\text{x}10^{-7}$
8S	N-LASF46B	121,000	6.846	18.500	43.846	39.000	$2.4\text{x}10^{-7}$
9S	N-SF14	88,000	7.379	18.500	44.379	42.000	$2.4\text{x}10^{-7}$
						Total	**$2.3\text{x}10^{-6}$**

Table 4. Bulk compliance of the 6061-T6 aluminum spacers in the stack computed with Equations 4.6 and 4.7 for v_{SPACER} = 0.33 and E_{SPACER} = 68,900 MPa.

Spacer	t_{SPACER} [mm]	OD_{SPACER} [mm]	$OD_{LENS\ 1}$ [mm]	$OD_{LENS\ 2}$ [mm]	y_{C1} [mm]	y_{C2} [mm]	C_{SPACER} [mm/N]
1S-2S	4.332	42.000	-	42.000	19.750	19.750	2.7E-07
2S-3S	2.000	42.000	-	-	18.500	18.500	9.4E-08
3S-4S	2.000	42.000	-	39.000	18.500	18.500	7.9E-08
4S-5S	2.000	42.000	39.000	-	18.500	18.500	7.9E-08
5S-6S	2.346	42.000	-	39.000	18.500	18.500	9.3E-08
6S-7S	2.813	42.000	39.000	-	18.500	18.500	1.1E-07
7S-8S	2.000	42.000	-	39.000	18.500	18.500	7.9E-08
8S-9S	15.894	42.000	39.000	-	18.500	18.500	6.3E-07
						Total	**$1.4\text{x}10^{-6}$**

5. COMPLIANCE IN ATHERMALIZED OPTICAL SYSTEMS

Given the bulk compliance analysis, the change in preload ΔP from the nominal assembly temperature (T_o = 20°C) to the maximum survival temperature (T_{max} = 120°C) is:

$$\Delta P = \frac{(\Delta T)(\alpha_{STACK} - \alpha_{BARREL})\sum_{i=1}^{n} t_i}{C_{BARREL} + \sum_{i=1}^{n} C_{LENSES} + \sum_{i=1}^{n} C_{SPACERS}} = \frac{(100°\text{C})(13.3\ \text{ppm/°C} - 23.6\ \text{ppm/°C})(84.961\ \text{mm})}{(2.9\text{x}10^{-6}\ \text{mm/N}) + (2.3\text{x}10^{-6}\ \text{mm/N}) + (1.4\text{x}10^{-6}\ \text{mm/N})} = -13,200\ \text{N}. \quad (5.1)$$

For a nominal preload of P = 45 N, the preload at the maximum survival temperature is $P_{120°C} = P + \Delta P$ = -13,155 N (effectively no preload retaining the lenses) and the preload at the minimum survival temperature is $P_{-80°C} = P - \Delta P$ = 13,245 N, a large enough force to crack all the lenses at the tangential spacer interfaces according to Equation 3.3.

The change in length between the barrel and the stack drives the large change in preload for this drop-in mechanical design. According to the numerator of Equation 5.1, a 6061-T6 aluminum barrel is 87.4 µm longer than the stack at the maximum survival temperature. To maintain a preload at T_{max} = 120°C, the preload at T_o = 20°C must compress the stack and the barrel by at least 87.4 µm. According to the denominator of Equation 5.1, the stack and the barrel (composed of bulk glass and metal) are very stiff. This combination of high stiffness and high deflection inevitably leads to high stress on the lenses.

One approach to mitigate the large change in preload is to add a spring to the stack [5]. From a static load perspective, the barrel, lenses, and spacers behave as springs in series with an overall compliance of $C_{OVERALL}$ = 6.6x10^{-6} mm/N. Turning one of the solid 6061-T6 aluminum spacers into a compliant spacer with $C_{SPRING} \approx$ 1x10^{-3} mm/N increases the overall compliance by three orders of magnitude, therefore reducing the change in preload from tens of thousands of Newtons to tens of Newtons.

A compliant spacer reduces the change in preload because it expands and contracts to compensate for the 87.4 µm change in length between the barrel and the stack. Since this deflection is different than the thermal expansion/contraction of a solid 6061-T6 aluminum spacer, the vertex to vertex spacing between the two lenses interfacing the compliant spacer varies differently with temperature than what we modelled for a solid spacer. For this reason, we derived an equation to calculate the effective CTE of the compliant spacer α_{SPRING} as:

$$\alpha_{SPRING} = \alpha_{SPACER} + \frac{\alpha_{BARREL} - \alpha_{STACK}}{t_{SPACER}} \sum_{i=1}^{n} t_i, \quad (5.2)$$

where t_{SPACER} and α_{SPACER} = 23.6 x10^{-6} ppm/°C are the length and CTE of the solid 6061-T6 spacer before being turned into a compliant spacer. The resulting effective CTEs of the compliant spacers are summarized in Table 5. Since the change in length with temperature of any spacer is proportional to its CTE and length, the effective CTE of the shorter spacers is larger than the effective CTE of the longer spacers.

Table 5. Effective CTEs of the compliant spacers computed with Equation 5.2 for Σt_i = 84.961 mm, α_{STACK} = 13.3 x10^{-6} ppm/°C, and α_{BARREL} = 23.6 x10^{-6} ppm/°C.

Spacer	t_{SPACER} [mm]	α_{SPRING} [ppm/°C]
Object-1S	-	-
1S-2S	4.332	225.4
2S-3S	2.000	460.7
3S-4S	2.000	460.7
4S-5S	2.000	460.7
5S-6S	2.346	396.2
6S-7S	2.813	334.4
7S-8S	2.000	460.7
8S-9S	15.894	78.6
9S-Image	29.000	53.7

We highlight that the effective CTEs of compliant spacers computed through Equation 5.2 and summarized in Table 5 apply only to their axial changes in length. The changes in the lens/spacer interface radial contact height are still governed by the CTE of the solid 6061-T6 aluminum spacers (α_{SPACER} = 23.6 x10^{-6} ppm/°C).

The impact of the effective CTE of compliant spacers on optical performance depends on the sensitivity of the optical system to the vertex to vertex spacing of its composing lenses at a given temperature. In 2020, we introduced a procedure to evaluate the effect of small spacer CTE perturbations (±5%) on the polychromatic RMS wavefront error of a passively athermalized optical system [8]. For this work, we adapted that method to evaluate the impact of the spacer CTE variations listed on Table 5 on the polychromatic MTF at 100 lp/mm. We show the sensitivity analysis results in Figure 5.

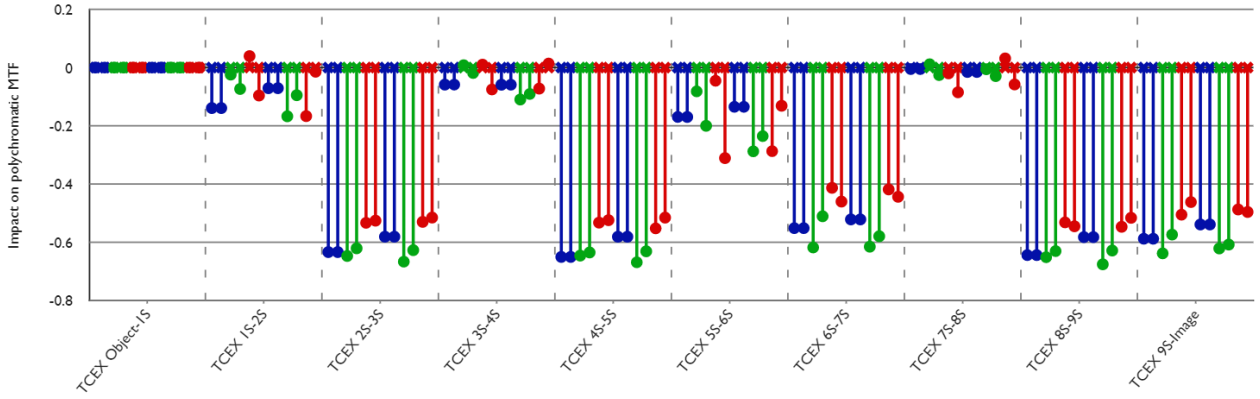

Figure 5. Sensitivity analysis of the effective CTE (TCEX) of compliant spacers on the sagittal and tangential polychromatic MTF at 100 lp/mm for T_{min} = -80°C and T_{max} = 120°C. Blue, green, and red data points represent the on-axis, 70% and 100% fields of view, respectively.

The only location for which the effective CTE of a compliant spacer has no impact on the optical performance of a passively athermalized optical system is between the retaining ring (or object) and the first lens. The sensitivity to the effective CTE varies greatly for all other spacers in the stack. For example, turning the 7S-8S spacer into a compliant spacer has almost no impact on the polychromatic MTF at T_{min} = -80°C and T_{max} = 120°C but turning the 8S-9S spacer into a compliant spacer degrades the polychromatic MTF to effectively zero at T_{min} = -80°C and T_{max} = 120°C.

Unfortunately, there are mechanical constraints that limit which spacers can be converted into compliant spacers. Specifically, the overall length constraint from the detector to the front surface of the barrel does not allow for enough space to add a spring between the retaining ring and the first lens. The TFL mount M35x0.75 mm thread on the interface between the barrel and the detector cannot be turned into a spring without damaging the threads. Furthermore, all the 2 mm thick, 42 mm diameter aluminum spacers are too fragile to be converted into compliant spacers. Given these mechanical constraints, the spacer between lenses eight and nine is the only suitable spacer for adding compliance as shown in the mechanical design layout in Figure 6.

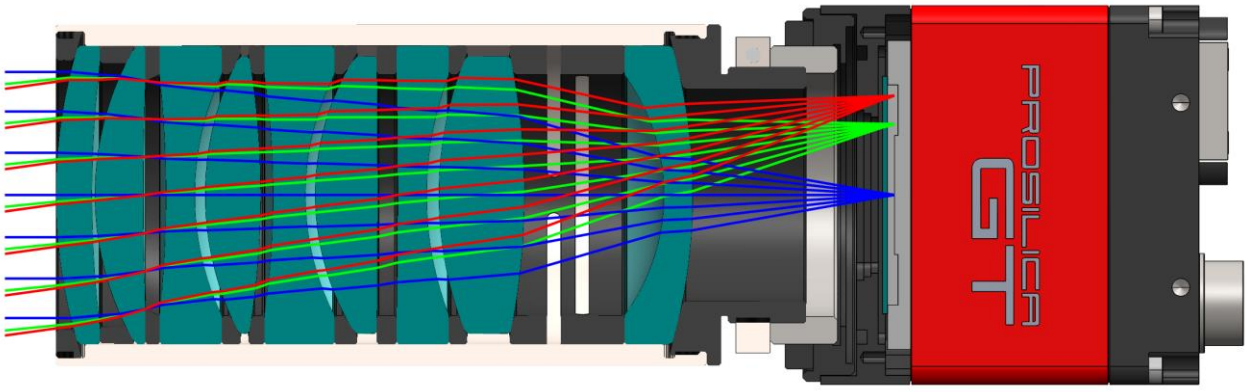

Figure 6. Mechanical design layout with a compliant spacer between lenses eight and nine. The blue, green and red rays represent the on-axis, 70% and 100% fields of view, respectively.

We performed a finite element analysis to estimate the stiffness of the compliant spacer shown in Figure 6. Fixing the conical surface that contacts the eighth lens and applying a 100 N force on the flat surface that contacts the ninth lens, we obtained a 200 µm deflection in the spacer length. From this result, we estimated the compliance to be C_{SPRING} = 2.0x10^{-3} mm/N, leading to a change in preload from T_o = 20°C to T_{max} = 120°C of:

$$\Delta P = \frac{(\Delta T)(\alpha_{STACK} - \alpha_{BARREL})\sum_{i=1}^{n} t_i}{C_{BARREL} + \sum_{i=1}^{n} C_{LENSES} + \sum_{i=1}^{n} C_{SPACERS}} = \frac{(100°C)(13.3\ \text{ppm/°C} - 23.6\ \text{ppm/°C})(84.961\ \text{mm})}{(2.9\text{x}10^{-6}\ \text{mm/N}) + (2.3\text{x}10^{-6}\ \text{mm/N}) + (2.0\text{x}10^{-3}\ \text{mm/N})} = -43.6\ \text{N}. \quad (5.3)$$

Substituting α_{SPRING} = 78.6 x10^{-6} ppm/°C for the CTE of the spacer between elements eight and nine yields the polychromatic MTF at T_{min} = -80°C, T_o = 20°C and T_{max} = 120°C shown in Figure 7. The poor optical performance at T_{min} = -80°C and T_{max} = 120°C is consistent with the results of the sensitivity analysis.

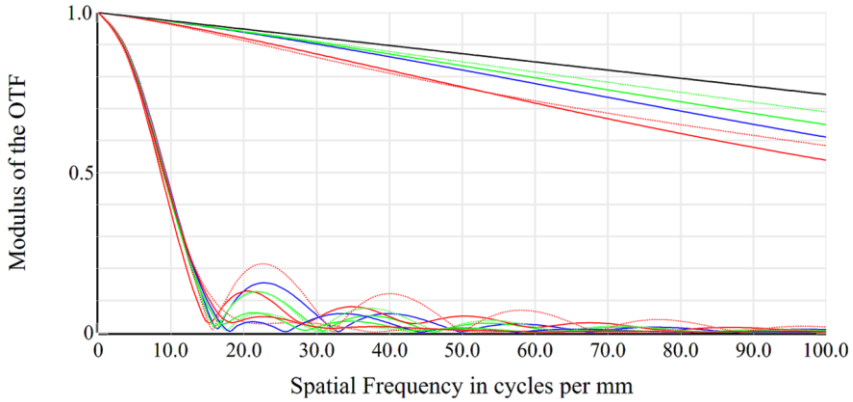

Figure 7. Polychromatic MTF overlay of the initial design with a 6061T6-Aluminum barrel and a compliant spacer between lenses eight and nine for T_{min} = -80°C, T_o = 20°C and T_{max} = 120°C. Blue, green, and red curves represent the on-axis, 70% and 100% fields of view, respectively.

6. BARREL MATERIAL SELECTION

Another approach to mitigate the large change in preload and effective CTE of the compliant spacer is to select a barrel material with CTE (α_{BARREL}) that better matches the overall CTE of the stack (α_{STACK} = 13.3 x10^{-6} ppm/°C). Figure 8 shows the 300 and 400 series stainless steels with CTEs closest to α_{STACK} [7]. The best match is 309-SS with α_{BARREL}= 14.9 x10^{-6} ppm/°C. Compared to the initial design, this barrel material substitution reduces the change in length between the barrel and the stack from 87.4 µm to 13.7 µm.

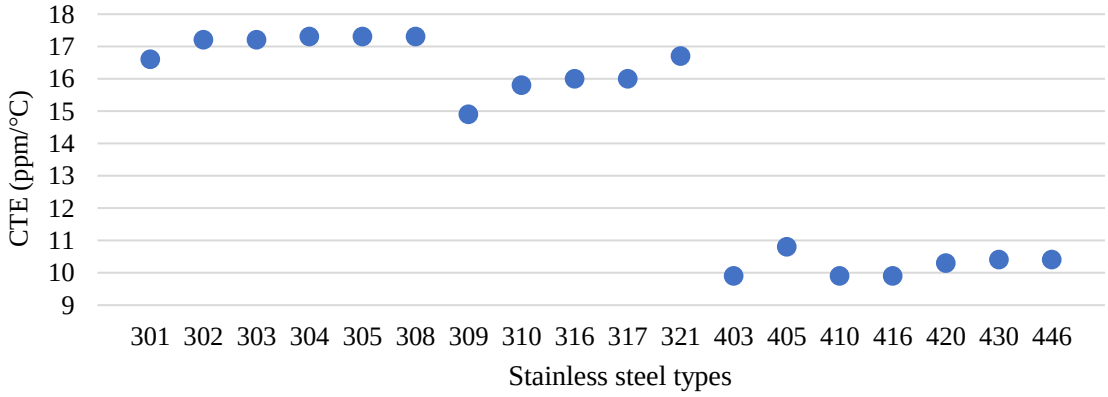

Figure 8. Coefficient of thermal expansion (CTE) of the 300 and 400 series stainless steels [7]. The closest steel CTE to CTE of the stack α_{STACK} = 13.3 x10^{-6} ppm/°C is α_{309SS} = 14.9 x10^{-6} ppm/°C.

The change in preload from the nominal assembly temperature (T_o = 20°C) to the maximum survival temperature (T_{max} = 120°C) for a 309-SS barrel is:

$$\Delta P = \frac{(\Delta T)(\alpha_{STACK} - \alpha_{BARREL})\sum_{i=1}^{n} t_i}{C_{BARREL} + \sum_{i=1}^{n} C_{LENSES} + \sum_{i=1}^{n} C_{SPACERS}} = \frac{(100°C)(13.3\ \text{ppm/°C} - 14.9\ \text{ppm/°C})(84.961\ \text{mm})}{(2.9\text{x}10^{-6}\ \text{mm/N}) + (2.3\text{x}10^{-6}\ \text{mm/N}) + (2.0\text{x}10^{-3}\ \text{mm/N})} = -6.9\ \text{N}. \quad (5.4)$$

Table 6 lists the resulting effective CTEs of the compliant spacers with a 309-SS barrel. The lower effective CTEs are consistent with the smaller change in length between the barrel and the stack.

Table 6. Effective CTEs of the compliant spacers computed with Equation 5.2 for Σt_i = 84.961 mm, α_{STACK} = 13.3 x10^{-6} ppm/°C, and α_{BARREL} = 14.9 x10^{-6} ppm/°C.

Spacer	t_{SPACER} [mm]	α_{SPRING} [ppm/°C]
Object-1S	-	-
1S-2S	4.332	55.3
2S-3S	2.000	92.3
3S-4S	2.000	92.3
4S-5S	2.000	92.3
5S-6S	2.346	82.1
6S-7S	2.813	72.4
7S-8S	2.000	92.3
8S-9S	15.894	32.2
9S-Image	29.000	28.3

Figure 9 shows the polychromatic MTF at T_{min} = -80°C, T_o = 20°C and T_{max} = 120°C for a 309-SS barrel and a compliant spacer between the eighth and ninth lenses. The lower effective CTE of the compliant spacer leads to an improvement in optical performance at T_{min} = -80°C and T_{max} = 120°C compared with the optical performance shown in Figure 7 for a 6061-T6 aluminum barrel and a larger compliant spacer effective CTE.

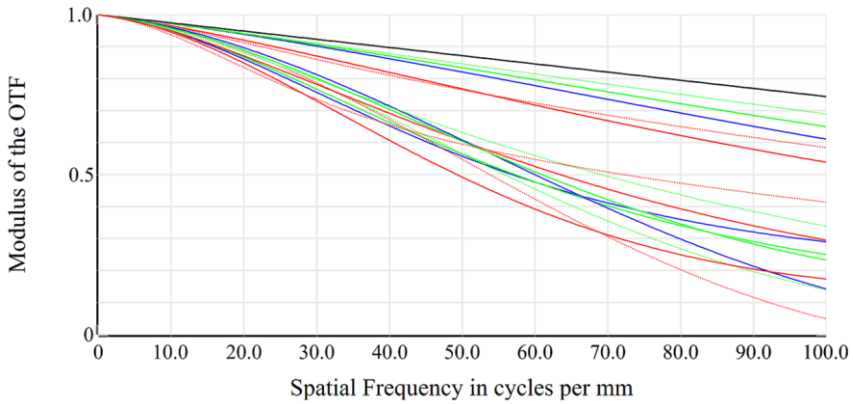

Figure 9. Polychromatic MTF overlay of the initial design with a 309 stainless steel barrel and a compliant spacer between lenses eight and nine for T_{min} = -80°C, T_o = 20°C and T_{max} = 120°C. Blue, green, and red curves represent the on-axis, 70% and 100% fields of view, respectively.

The combination of a 309-SS barrel and a compliant spacer between the eighth and ninth lenses results in a small change in preload ΔP = -6.9 N. For a larger nominal preload of P = 55 N, the minimum preload at the maximum survival temperature is $(P_{120°C})_{MIN} = P - P_{AXIAL} + \Delta P$ = 18 N (enough to retain the lenses under axial acceleration) and the maximum preload at the minimum survival temperature is $(P_{-80°C})_{MAX} = P - P_{AXIAL} - \Delta P$ = 92 N, which still allows for a large factor of safety in the contact stress at the tangential spacer interfaces according to Equation 3.3. However, the effective CTE of the compliant spacer degrades the polychromatic MTF beyond the minimum MTF specification of 40% at 100 lp/mm.

7. OPTIMIZATION FOR BARREL MATERIAL

The last approach to mitigate the large change in preload and effective CTE of the compliant spacer is to reoptimize the optical design to match the overall CTE of the stack to the CTE of the closest available barrel material α_{BARREL} = 14.9 x10^{-6} ppm/°C. To do so, we first calculated the overall CTE of the stack in optical design software through Equation 4.2 using dummy surfaces to compute the length of the lenses and spacers at their contact heights. We then reoptimized the design for α_{STACK} - α_{BARREL} = 0. In this way, the CTE of the barrel is accounted for in a similar way as other mechanical constraints such as the maximum overall length from the detector to the front surface of the barrel, minimum lens thickness, minimum spacer thickness, etc. Figure 10 shows the optical design layout of the reoptimized design. Compared to the initial design shown in Figure 1, the thicknesses of the lenses at the spacer contact heights decreased and the lengths of the spacers increased to achieve the increase in stack CTE from 13.3 x10^{-6} ppm/°C to 14.9 x10^{-6} ppm/°C.

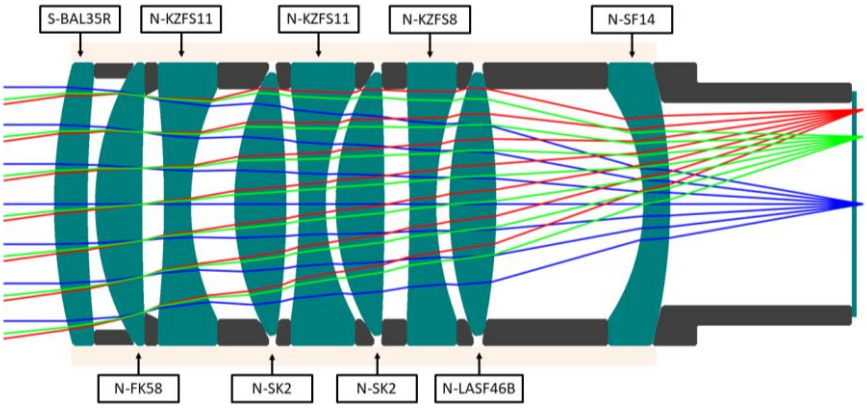

Figure 10. Reoptimized optical design layout with a 309-SS barrel and 6061-T6 aluminum spacers.

Figure 11 shows the polychromatic MTF of the reoptimized design with a 309-SS barrel for T_{min} = -80°C, T_o = 20°C and T_{max} = 120°C. Adding the stack CTE constraint to the merit function had a negligible impact on optical performance.

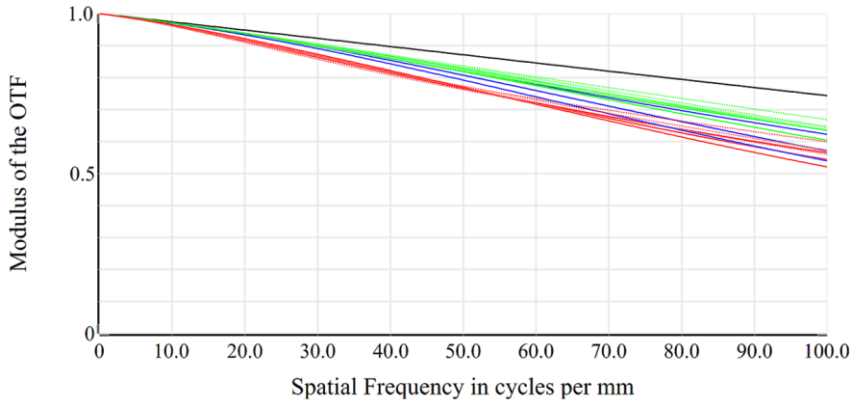

Figure 11. Polychromatic MTF overlay of the reoptimized design with a 309-SS barrel for T_{min} = -80°C, T_o = 20°C and T_{max} = 120°C. Blue, green, and red curves represent the on-axis, 70% and 100% fields of view, respectively.

According to Equation 4.1, the preload does not change with temperature when (α_{STACK} - α_{BARREL} = 0). Consequently, the reoptimized design should not need a compliant spacer. However, the CTEs of the glasses and metals in the stack and barrel inevitably vary between production runs. These CTE values are commonly reported to one significant figure with no tolerance information in their respective catalogs. Furthermore, the glass CTE for a specific melt is generally not included in the melt data report with the glass refractive index measured at multiple wavelengths. For this reason, we perturb the thermo-optical coefficients and CTEs of glasses and the CTEs of metals in our optical performance tolerance analysis of passively athermalized optical systems [8]. Extending this sensitivity analysis to the mechanical domain, we found that in the absence of a compliant spacer in the stack, a ±5% variation in the CTE of the barrel or stack leads to a change in preload from the nominal assembly temperature (T_o = 20°C) to the maximum survival temperature (T_{max} = 120°C) of:

$$\Delta P = \frac{(\Delta T)(\alpha_{STACK})(1.05)\sum_{i=1}^{n} t_i}{C_{BARREL} + \sum_{i=1}^{n} C_{LENSES} + \sum_{i=1}^{n} C_{SPACERS}} = \frac{(100°\text{C})(14.9\ \text{ppm/°C})(1.05)(86.720\ \text{mm})}{(3.0\text{x}10^{-6}\ \text{mm/N}) + (2.1\text{x}10^{-6}\ \text{mm/N}) + (1.8\text{x}10^{-6}\ \text{mm/N})} = -937\ \text{N}, \quad (7.1)$$

where the stack length Σt_i = 86.720 mm, α_{STACK} = 14.9 x10^{-6} ppm/°C, C_{BARREL} = 3.0x10^{-6} mm/N, ΣC_{LENSES} = 2.1x10^{-6} mm/N, and $\Sigma C_{SPACERS}$ = 1.8x10^{-6} mm/N values were updated according to the bulk compliance analysis presented in section 4. Based on this result, it is still necessary to include a compliant spacer in the stack even when the overall CTE of the stack is designed to match the nominal CTE of the barrel. Figure 12 shows the mechanical design layout of the reoptimized system with a compliant spacer with effective CTE α_{SPRING} = 27.1 x10^{-6} ppm/°C between the eighth and ninth lenses to account for a ±5% uncertainty on the catalog CTE values.

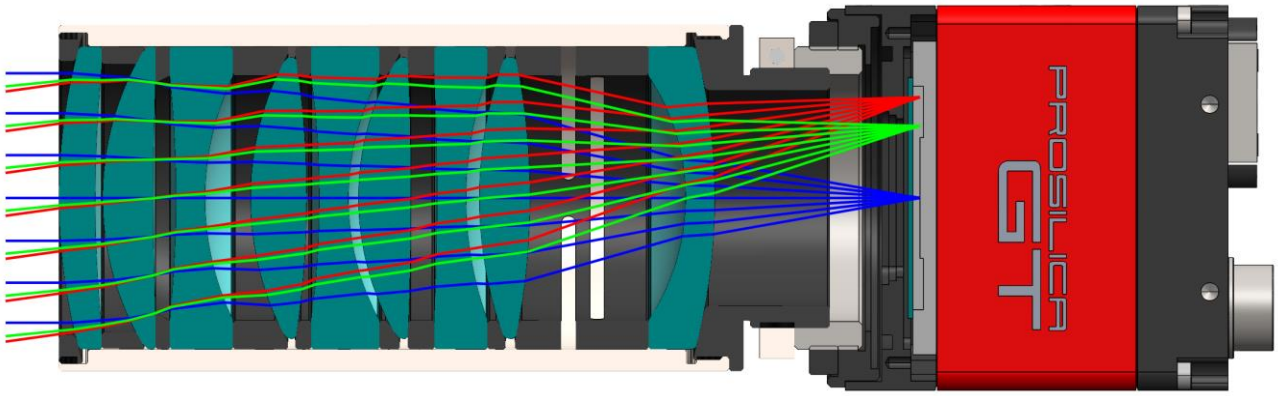

Figure 12. Reoptimized mechanical design layout with a 309-SS barrel and a compliant spacer between lenses eight and nine. The blue, green and red rays represent the on-axis, 70% and 100% fields of view, respectively.

Figure 13 shows the polychromatic MTF of the reoptimized design with a 309-SS barrel and a compliant spacer between lenses eight and nine for T_{min} = -80°C, T_o = 20°C and T_{max} = 120°C. The optical performance slightly decreased, as expected when tolerancing an optical system. However, the polychromatic MTF still meets the minimum MTF specification of 40% at 100 lp/mm for a ±5% variation in the CTE of the barrel or stack.

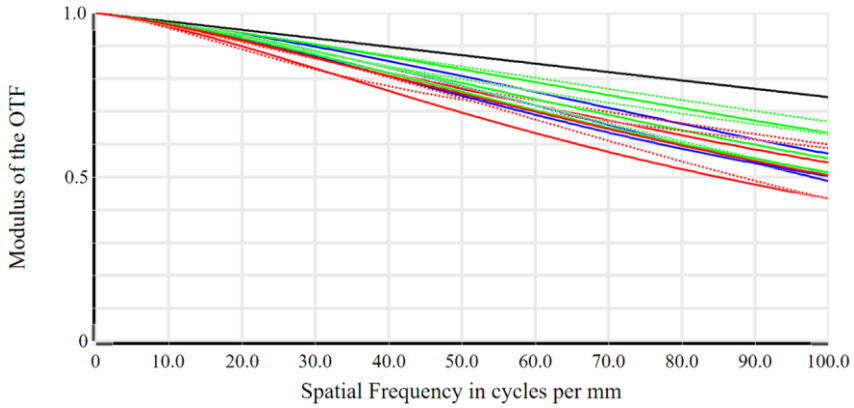

Figure 13. Polychromatic MTF overlay of the reoptimized design with a 309-SS barrel and a compliant spacer between lenses eight and nine for T_{min} = -80°C, T_o = 20°C and T_{max} = 120°C. Blue, green, and red curves represent the on-axis, 70% and 100% fields of view, respectively.

8. CONCLUSIONS

We studied the impact of the barrel material on the polychromatic MTF of a drop-in passively athermalized optical system. We showed that a mismatch between the CTE of the barrel and the overall CTE of the lens stack can lead to a large change in length between the barrel and the stack at the maximum survival temperature. Given the high stiffness of the barrel, lenses, and spacers, this change in length results in a large change in the preload force retaining the lenses.

We considered three approaches to mitigate this issue: turning one of the spacers into a compliant spacer, selecting the barrel material that best matches the overall CTE of the lens stack, and reoptimizing the optical system to nominally match the overall CTE of the lens stack to the CTE of the barrel.

We explained how a compliant spacer reduces the change in preload by expanding to compensate for the change in length between the barrel and the stack. Since this deflection is different than the thermal expansion of a solid spacer, we provided an equation to calculate its effective CTE and evaluated its detrimental impact on the polychromatic MTF at different environmental conditions. To minimize the performance degradation, we substituted the barrel material for a better match with the overall CTE of the stack. Despite a smaller change in length between the barrel and the stack, a compliant spacer was still necessary to minimize the change in preload and the polychromatic MTF was still below the specification.

Reoptimizing the design to account for the barrel material by matching the overall CTE of the stack to the CTE of the barrel yielded a similar polychromatic MTF to the initial design and nominally zero change in the preload retaining the lenses. However, a compliant spacer was still necessary to prevent a large change in preload due to the uncertainty of the CTE values of the glass and metal catalogs. Its impact on optical performance was comparable to other lens tolerances.

The drop-in mounting scheme considered in this work is neither the only nor the best way to mount the lenses in this optical system. Drop-in mounting tolerances are most certainly too loose for the as-built system to meet the minimum MTF specification. Nonetheless, the mechanical analysis of this drop-in passively athermalized optical system highlights the predicament of mounting lenses that were not optimized for best optical and best mechanical performance. The tools available to optomechanical engineers (adding compliance and substituting the barrel material) are most effective when used in conjunction with the optimization capabilities of optical design software.

REFERENCES

[1] Bach, H., and Neuroth N., The Properties of Optical Glass. Springer, 1998.

[2] Schott, “Temperature Coefficient of the Refractive Index” Schott Technical Information TIE-19 (2008)

[3] Schott, “Refractive index and Dispersion” Schott Technical Information TIE-29 (2007)

[4] Rogers, J. R., "Passive athermalization: Required accuracy of the thermo-optical coefficients,” Proc. SPIE 9293, 92931A (2014).

[5] Yoder, P., and Vukobratovich D. Opto-Mechanical Systems Design, Fourth Edition, Volume 1: Design and Analysis of Opto-Mechanical Assemblies. CRC Press, 2015.

[6] Genberg, V.L., Structural analysis of optics, in *Handbook of Optomechanical Engineering*, Ahmad, A., Ed., CRC Press, Boca Raton, FL, 1997a, Chapter 8.

[7] “Online Materials Information Resource.” MatWeb, https://www.matweb.com/index.aspx.

[8] Tangari Larrategui, M., Densmore III, V. E., Johnson, L., Giokaris, C., Medicus, K., Castle, K. R., and Stuhlinger, T. W. "Sensitivity analysis of the CTE and thermo-optical coefficients of a passively athermalized lens", Proc. SPIE 11488, 1148809 (2020).

APPENDIX

The prescriptions of the initial and reoptimized designs are summarized in Tables A1 and A2.

Table A1. Initial design

Surface	Radius, R [mm]	Thickness, t (mm)	Material	Contact height, y_C [mm]	Contact type
1S_s1	73.063	5.000	S-BAL35R	20.000	Surface
1S_s2	149.927	0.501		18.500	Annulus
2S_s1	41.676	6.750	N-FK58	19.750	Surface
2S_s2	428.949	0.337	-	17.000	Annulus
STOP	Infinity	2.923	-	-	Annulus
3S_s1	-157.051	4.000	N-KZFS11	17.000	Annulus
3S_s2	39.901	1.534	-	17.000	Annulus
4S_s1	42.223	7.750	N-SK2	18.500	Surface
4S_s2	-118.794	1.817	-	18.500	Surface
5S_s1	-114.770	4.500	N-KZFS11	17.000	Annulus
5S_s2	37.329	1.439	-	17.000	Annulus
6S_s1	36.705	8.750	N-SK2	18.500	Surface
6S_s2	-1574.081	2.893	-	18.500	Surface
7S_s1	-765.228	4.000	N-KZFS8	17.000	Annulus
7S_s2	47.173	1.774	-	17.000	Annulus
8S_s1	52.091	12.000	N-LASF46B	18.500	Surface
8S_s2	-98.196	19.750	-	18.500	Surface
9S_s1	-28.543	4.000	N-SF14	17.000	Annulus
9S_s2	-77.657	26.764	-	18.500	Surface
10W_s1	Infinity	0.700	K10	15.000	Annulus
10W_s2	Infinity	1.000	-	15.000	Annulus
Image	Infinity	-	-	-	-

Table A2. Reoptimized design

Surface	Radius, R [mm]	Thickness, t (mm)	Material	Contact height, y_C [mm]	Contact type
1S_s1	80.598	5.000	S-BAL35R	20.000	Surface
1S_s2	183.199	1.096		18.500	Annulus
2S_s1	39.835	7.000	N-FK58	19.750	Surface
2S_s2	442.730	0.327	-	17.000	Annulus
STOP	Infinity	2.883	-	-	Annulus
3S_s1	-164.053	4.000	N-KZFS11	17.000	Annulus
3S_s2	38.840	6.395	-	17.000	Annulus
4S_s1	41.038	7.750	N-SK2	18.500	Surface
4S_s2	-128.012	1.828	-	18.500	Surface
5S_s1	-123.850	4.000	N-KZFS11	17.000	Annulus
5S_s2	35.568	1.461	-	17.000	Annulus
6S_s1	37.612	7.250	N-SK2	18.500	Surface
6S_s2	-439.559	3.670	-	18.500	Surface
7S_s1	-368.573	4.000	N-KZFS8	17.000	Annulus
7S_s2	49.375	1.911	-	17.000	Annulus
8S_s1	56.621	7.000	N-LASF46B	18.500	Surface
8S_s2	-97.272	21.748	-	18.500	Surface
9S_s1	-30.387	4.000	N-SF14	17.000	Annulus
9S_s2	-83.384	26.922	-	18.500	Surface
10W_s1	Infinity	0.700	K10	15.000	Annulus
10W_s2	Infinity	1.000	-	15.000	Annulus
Image	Infinity	-	-	-	-